nature astronomy

SUPPLEMENTARY INFORMATION

https://doi.org/10.1038/s41550-020-1092-5

In the format provided by the authors and unedited.

Evidence of extensive lunar crust formation in impact melt sheets 4,330 Myr ago

L. F. White[1,2] ✉, A. Černok[1,2,3], J. R. Darling[4], M. J. Whitehouse[5], K. H. Joy[6], C. Cayron[7], J. Dunlop[4], K. T. Tait[1,2] and M. Anand[3,8]

[1]Centre of Applied Planetary Mineralogy, Department of Natural History, Royal Ontario Museum, Toronto, Ontario, Canada. [2]Department of Earth Sciences, University of Toronto, Toronto, Ontario, Canada. [3]School of Physical Sciences, The Open University, Milton Keynes, UK. [4]School of Earth and Environmental Sciences, University of Portsmouth, Portsmouth, UK. [5]Swedish Museum of Natural History, Stockholm, Sweden. [6]Department of Earth and Environmental Science, University of Manchester, Manchester, UK. [7]Laboratory of ThermoMechanical Metallurgy (LMTM), PX Group Chair, École Polytechnique Fédérale de Lausanne (EPFL), Neuchâtel, Switzerland. [8]Department of Earth Sciences, The Natural History Museum, London, UK.
✉e-mail: lwhite@rom.on.ca

Evidence of extensive lunar crust formation in impact melt sheets 4330 Myr ago

White, L. F[1,2*], Černok, A[1,2,3], Darling, J. R[4], Whitehouse, M.J. [5], Joy, K. H.[6], Cayron, C[7], Dunlop, J[4], Tait, K. T[1,2] & Anand, M[3,8].

[1]*Centre of Applied Planetary Mineralogy, Department of Natural History, Royal Ontario Museum, Toronto, Ontario, M5S 2C6, Canada.*

[2]*Department of Earth Sciences, University of Toronto, Toronto, Ontario, M5S 3B1, Canada.*

[3]*School of Physical Sciences, The Open University, Milton Keynes, MK7 6AA, UK.*

[4]*School of Earth and Environmental Sciences, Burnaby Building, Burnaby Road, University of Portsmouth, Portsmouth, PO1 3QL, UK.*

[5]*Swedish Museum of Natural History, Box 50007, SE-104 05 Stockholm, Sweden*

[6]*School of Earth and Environmental Science, University of Manchester, Oxford Road, Manchester, M13 9PL, UK.*

[7]*Laboratory of ThermoMechanical Metallurgy (LMTM), École Polytechnique Fédérale de Lausanne (EPFL), Rue de la Maladière 71b,2000 Neuchâtel, Switzerland.*

[8]*Department of Earth Sciences, The Natural History Museum, Cromwell Road, London, SW7 5BD, UK.*

**Corresponding author: lwhite@rom.on.ca*

Supplementary Materials:

Supplementary Figure 1: Raw EBSD data for baddeleyite and feldspar.

Supplementary Figure 2: Operator statistics (A), pole figure diagrams (B,C) and reconstructed tetragonal-ZrO_2 packets (D) incorporated into reconstruction of a single cubic parent grain.

Supplementary Figure 3: Target SIMS locations superimposed onto EBSD map of large baddeleyite grain in troctolite 76535.

Supplementary Table 1: Chronological list of events leading to the observed baddeleyite structure and age data.

Supplementary Table 2: All electron probe microanalysis (EPMA) chemical data for twelve analysis spots on the large baddeleyite grain located in Apollo troctolite 76535.

Supplementary Table 3: Pb-Pb age data for large, microstructurally complex baddeleyite grain in Apollo troctolite 76535.

Supplementary Table 4: Modelled influence of common lead corrections on the measured Pb-Pb age for baddeleyite grain in Apollo troctolite 76535.

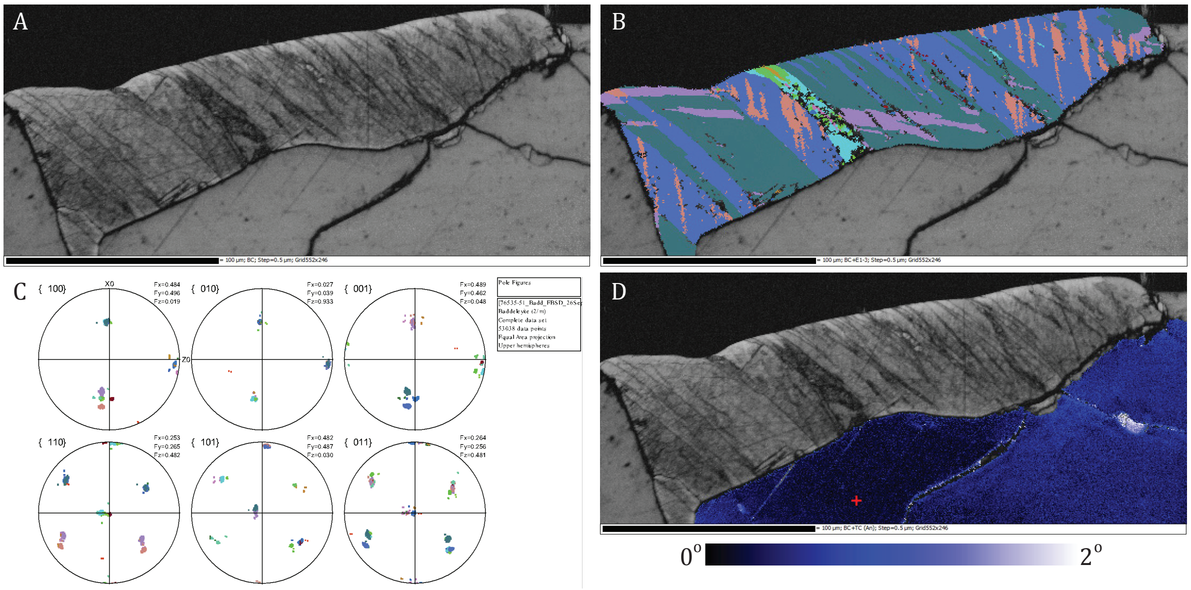

Supplementary Figure 1: Raw EBSD data for baddeleyite and feldspar. *All baddeleyite indexes as monoclinic-ZrO_2, indicating no preservation of the parent tetragonal or cubic phase. Reversion domains can be observed in band contrast imaging of the grain (**A**), which reveals a range of crystallinity between regions. All-Euler imaging of the grain (**B**) displays the crystal orientations (**C**), which yield orthogonally (90°) related clusters in all pole directions. EBSD mapping of the surrounding feldspar grain (**D**) reveals less than 1° of crystal plastic deformation, highlighting an absence of shock deformation of the sample.*

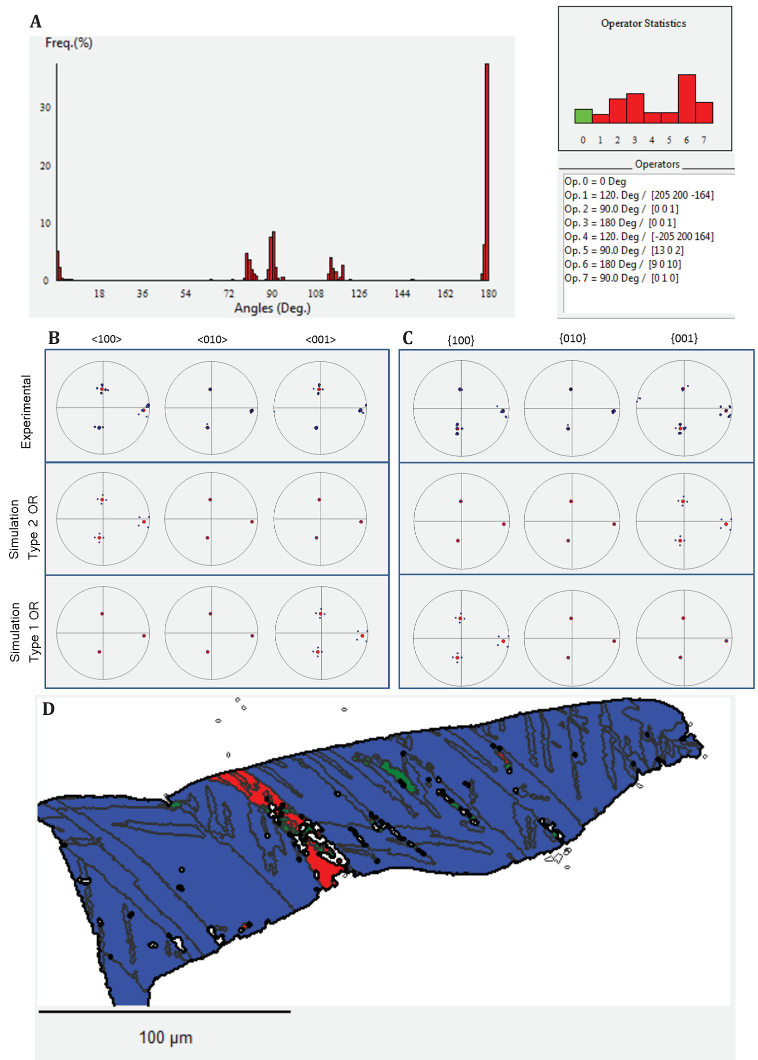

Supplementary Figure 2: Operator statistics (A), pole figure diagrams (B,C) and reconstructed tetragonal-ZrO_2 packets (D) incorporated into reconstruction of a single cubic parent grain. *Operator statistics (**A**) reveal peaks in disorientation at 90°, 120° and 180° between the monoclinic variants inherited from a cubic crystal via Type 2 OR. The peaks at 80° and 115° can be attributed to misorientations between variants in Type 1 OR and those in Type 2 OR. The cubic-monoclinic heritage is further strengthened by the presence of three unique crystallographic axes in the <010> (b-axis) directions along the three <100> cubic directions of the prior cubic grain, as shown by the stereographic pole figures of the <100>, <010> and <001> directions (**B**) and {100}, {010} and {001} planes (**C**). The pole figures are simulated with the software GenOVa[33] with Type 2 OR and Type 1 OR in second and third line of (**B,C**), respectively. The pole figures cannot be explained by reversion from the tetragonal or orthorhombic systems alone[2]. To localize the intermediate tetragonal domains, the 12 monoclinic variants inherited from the cubic grains were partitioned into three packets of four variants sharing the same b-axis oriented along the same <100> c-axis (**D**). The analysis reveals that one b-packet dominates the two others, which proves that a majority (but not all) the baddeleyite grains come from a unique prior tetragonal domain (blue domains in **D**) crossed by a second large tetragonal domain (red) and smaller third domains (green). The unique orientations of these tetragonal precursors can be correlated with a single cubic parent (i.e. Figure 1c).*

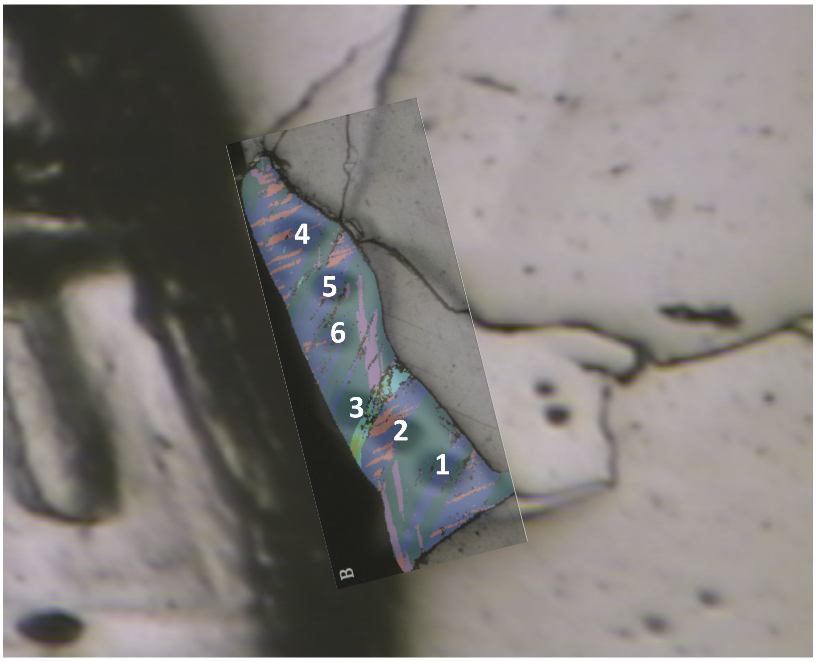

Supplementary Figure 3: Target SIMS locations on large baddeleyite grain in troctolite 76535 with raw all euler EBSD map superimposed for reference. *The youngest Pb-Pb ages are reported from SIMS spots located on densely twinned domains (i.e. spot 3), while the oldest ages are reported from more cohesive crystallographic regions (i.e. spots 1 and 4).*

Event	ZrO_2 Structure	Temp	Age	Inferred process
Crystallization of baddeleyite from initial lunar magma	***m*-ZrO_2**	< 900 °C	> 4334.1 ± 2.1 Mya	Giant impact -> LMO crystallization / mantle overturn
Transformation to cubic-ZrO_2	***c*-ZrO_2**	~2300 °C	4326 ± 16 Mya	Incorporation into large, super-heated impact melt basin
Reversion to monoclinic-ZrO_2	**Reverted *m*-ZrO_2**	2300 -> 900 °C	4299.5 ± 4.4	Partial to complete Pb loss during melt sheet cooling
Fresh baddeleyite growth as small matrix grains	**Reverted *m*-ZrO_2** + Fresh *m*-ZrO_2	< 900 °C	4271 ± 29 Mya	Final impact melt crystallization below < 900 deg C (closure temp of badd)
Argon closure of rock	**Reverted *m*-ZrO_2** + Fresh *m*-ZrO_2	~350 °C	4249 ± 12 Mya	Final cooling of impact melt crystallization

Supplementary Table 1: Chronological list of events leading to the observed baddeleyite structure and age data. *For each 'event', the observed ZrO_2 structure, estimated temperature, estimated age and inferred process as detailed to aid interpretation of the P-T-t history of Apollo troctolite 76535.*

wt% oxide	MgO	CaO	FeO	Al_2O_3	SiO_2	TiO_2	ZrO_2	HfO_2	Total
	0.06	0.14	0.08	0.04	0.09	1.67	94.62	1.39	98.09
	0.03	0.03	0.02	0.03	0.09	1.17	96.2	1.36	98.91
	0.02	0.04	0.04	0.01	0.08	1.29	95.47	1.49	98.44
	0.03	0.02	0.01	0	0.09	1.28	95.13	1.42	97.98
	0.02	0.04	0	0.01	0.07	1.25	95.32	1.4	98.12
	0.04	0.02	0.03	0	0.09	1.22	96.28	1.36	99.05
	0.02	0.04	0	0.01	0.07	1.31	95.77	1.37	98.58
	0.02	0.03	0.02	0	0.07	1.24	95.89	1.33	98.58
	0.03	0.01	0.02	0.01	0.06	1.19	95.78	1.45	98.54
	0.02	0.02	0.01	0	0.09	1.23	96.06	1.38	98.82
	0.03	0.04	0	0.01	0.1	1.28	95.4	1.45	98.3
	0.01	0.02	0.01	0	0.07	0.95	96.15	1.41	98.62
Average	0.03	0.04	0.02	0.01	0.08	1.26	95.67	1.4	98.5
Std Dev	0.01	0.03	0.02	0.01	0.01	0.16	0.5	0.05	0.33

Supplementary Table 2: All electron probe microanalysis (EPMA) chemical data for twelve analysis spots on the large baddeleyite grain located in Apollo troctolite 76535. *For reference, average and standard deviation values are reported for all species.*

Sample #	$^{207}Pb/^{206}Pb$	±σ %	$^{208}Pb/^{206}Pb$	±σ %	$^{204}Pb/^{206}Pb$ *meas*	±σ %	f_{206}%	Age *(Ma)*	± err
76535,51_190214_@4	**0.53260**	**0.14**	**0.04486**	**1.2**	**0.000003**	**15.1**	**0.006**	**4334.1**	**2.1**
76535,51_190214_@1	**0.53189**	**0.13**	**0.04191**	**0.3**	**0.000002**	**16.9**	**0.004**	**4332.1**	**1.9**
76535,51_190214_@6	**0.53064**	**0.17**	**0.04368**	**0.6**	**0.000005**	**11.4**	**0.009**	**4328.7**	**2.4**
76535,51_190214_@2	**0.53020**	**0.12**	**0.04799**	**1.1**	**0.000002**	**21.8**	**0.003**	**4327.5**	**1.8**
76535,51_190214_@5	**0.52864**	**0.16**	**0.04589**	**2.4**	**0.000004**	**11.5**	**0.007**	**4323.1**	**2.4**
76535,51_190214_@3	**0.52020**	**0.30**	**0.04159**	**5.9**	**0.000002**	**20.0**	**0.004**	**4299.5**	**4.4**

Supplementary Table 3: Pb-Pb age data for large, microstructurally complex baddeleyite grain in Apollo troctolite 76535. *Spot numbers (@1-@6) correlate with spots 1-6 on labelled Supplementary Figure 3.*

		model initials (mu3 = 0)			*sec. isochron, mu3 = 50*			
	SK 0 Ma terrestrial	***mu2=400***	***mu2 = 1000***	***mu2 = 2000***	***mu2=400***	***mu2 = 1000***	***mu2 = 2000***	
206Pb/204Pb	18.703	32.440	42.672	59.725	80.166	90.397	107.450	
207Pb/206Pb	0.8356	1.5951	1.6198	1.6422	0.9595	1.0431	1.1471	
Sample/ spot #	**Age *(Ma)***	**Age *(Ma)***	**Age *(Ma)***	**Age *(Ma)***	**Age *(Ma)***	**Age *(Ma)***	**Age *(Ma)***	**Max. age shift**
76535,51_190214_@1	4338.6	4338.4	4338.3	4338.2	4338.4	4338.3	4338.2	0.4
76535,51_190214_@2	4333.9	4333.8	4333.7	4333.6	4333.8	4333.7	4333.6	0.3
76535,51_190214_@3	4306.0	4305.8	4305.7	4305.6	4305.8	4305.7	4305.6	0.4
76535,51_190214_@4	4340.5	4340.2	4340.1	4340.0	4340.2	4340.1	4340.0	0.6
76535,51_190214_@5	4329.6	4329.3	4329.1	4328.9	4329.3	4329.1	4328.9	0.6
76535,51_190214_@6	4335.1	4334.8	4334.6	4334.4	4334.8	4334.6	4334.4	0.8
average	**4330.6**	**4330.4**	**4330.3**	**4330.1**	**4330.4**	**4330.3**	**4330.1**	0.5
sd	**12.7**	**12.6**	**12.6**	**12.6**	**12.6**	**12.6**	**12.6**	

Supplementary Table 4: Modelled influence of common lead corrections on the measured Pb-Pb age for baddeleyite grain in Apollo troctolite 76535. *The influence of terrestrial common Pb (0 Ma), lunar common lead introduced to the baddeleyite at the time of crystallization (~4.3 Ga) from basalt-like (400 $\mu 2$) to KREEP-like (1000 and 2000 $\mu 2$) sources. Mixing of these common lead sources (50 $\mu 3$) to model contamination from surrounding phases (such as feldspar) is also presented from a range of lunar sources. In all scenarios, a maximum shift in the Pb-Pb age of 0.8 Ma is observed, showing that common lead has a minimal influence on the calculated age of the grain.*